Bulletin of Volcanology (2023) 85:10
https://doi.org/10.1007/s00445-022-01622-z

RESEARCH ARTICLE

Evolving shallow conduit revealed by tremor and vent activity observations during episodic lava fountaining of the 2021 Geldingadalir eruption, Iceland

Eva P. S. Eibl[1] · Thor Thordarson[2] · Ármann Höskuldsson[2] · Egill Á. Gudnason[3] · Thoralf Dietrich[1] · Gylfi Páll Hersir[4] · Thorbjörg Ágústsdóttir[3]

Received: 10 March 2022 / Accepted: 22 November 2022

Abstract

Cyclic behaviour is observed in volcanic phenomena ranging from caldera collapses to explosions, spattering or lava fountaining. The repeating processes can define irregular, regular or systematically changing patterns. These patterns yield information about the subsurface structure, which often is not considered in detail. We analyse the pattern of 7058 lava fountaining episodes that occur between 2 May and 14 June 2021 during the Geldingadalir eruption, Iceland. Our seismometer records the lava fountaining episodes as tremor episodes. We analyse the seismic tremor amplitude, the episode duration, the repose time and the sum of episode duration and repose time (cycle duration). We define six periods characterised by different patterns: Three periods feature long episodes that exponentially shorten with time. One period features coexisting long and short episodes in a haphazard sequence. One period shows a stable pulsing duration but increasing repose time, and one period has stable, short episodes and repose times. We conclude that the episodic fountaining starts because a shallow-conduit container forms on 2 May shifting the magma degassing from sustained continuous to an episodic state. This situation evolves until 11 May when a semi-stable state is reached. The length of the repose times is most likely influenced by the amount of outgassed magma present in the uppermost part of the shallow conduit. Finally, we suggest that the vent is mechanically eroded and widens with time causing increasing seismic tremor amplitudes. However, the trends are frequently punctuated by partial crater wall collapses that temporarily disrupt the system.

Keywords Seismology · Volcanic tremor · Crater collapses · Magma viscosity · Lava fountaining · Vent evolution

Main findings

- Our seismometer recorded 7058 lava fountain episodes of the Geldingadalir eruption, Iceland, between 2 May and 14 June 2021.
- We define six periods with distinct fountaining patterns featuring fast changing episode duration, stable episode duration and coexisting short and long episodes.
- The pattern is affected by processes such as an evolving shallow-conduit container from 2 to 11 May, crater rim collapses, accumulating degassed magma and the vent dimensions.

Introduction

Tremor is an emergent, long-lasting volcano-seismic signal that precedes and accompanies eruptions and magmatic activity (Zobin 2017). It can serve to distinguish sources and

Editorial responsibility: F. Sigmundsson; Deputy Executive Editor: L. Pioli

This paper constitutes part of a topical collection: *Low intensity basalt eruptions: the 2021 Geldingadalir and 2022 Meradalir eruptions of the Fagradalsfjall Fires, SW Iceland*

✉ Eva P. S. Eibl
eva.eibl@uni-potsdam.de

[1] Institute for Geosciences, University of Potsdam, Karl-Liebknecht-Str. 24/25, Potsdam-Golm, Germany

[2] University of Iceland, Sturlugata, Reykjavik, Iceland

[3] ISOR, Iceland GeoSurvey, Urdarhvarf 8, Reykjavik, Iceland

[4] Independent researcher, Reykjavik, Iceland

Published online: 23 January 2023

eruptive activity styles (Falsaperla et al. 2005; Langer et al. 2009) for example when the eruption is obscured by poor visibility. While tremor can persist for years (Cannata et al. 2008; Swanson et al. 1979), it can also transition to a start and stop behaviour (Eibl et al. 2017a) or appear episodically (Andronico et al. 2021; Heliker and Mattox 2003; Patrick et al. 2011; Privitera et al. 2003; Thompson et al. 2002; Zobin 2013).

Cyclic behaviour occurs in different volcanic contexts ranging from caldera collapses to explosions, spattering or lava fountaining. Caldera collapses are often composed of several collapse events recorded as tremor episodes (Michon et al. 2007), repeating volcano-tectonic earthquakes (Gudmundsson et al. 2016; Tepp et al. 2020) or VLP earthquakes (Kumagai et al. 2001). For example, pulsatory eruptions can be temporarily typified by a series of overlapping explosion bursts (Dominguez et al. 2016). Fast repeating explosion patterns are also detected near erupting geysers (Azzalini and Bowman 1990; Eibl et al. 2020; Munoz-Saez et al. 2015) where steam bubbles reach the surface and expel boiling water into the air. A perched lava channel can exhibit a cyclic pattern of lava level rise and spattering (Patrick et al. 2011). Finally, a sharp tremor increase has been observed to accompany lava fountaining at volcanoes worldwide (e.g. (Alparone et al. 2003; Falsaperla et al. 2005; Heliker and Mattox 2003; La Spina et al. 2015; McNutt 1987; Privitera et al. 2003; Tanguy and Patane 1984)).

Independent of these different contexts, tremor episodes can occur in regular, irregular or systematically changing intervals. Stable repose times around 24 h with rare fluctuations up to 120 h and down to 8.4 h were reported at Pu'u 'Ō'ō from 1983 to 1986 (Heliker and Mattox 2003). Privitera et al. (2003) reported cyclic lava fountaining on Etna in 1989 and successfully posteriori forecasted some eruptions using simple statistical methods. Based on 73466 eruptions, Eibl et al. (2020) concluded that Strokkur geyser in south Iceland erupts on average every 3.7±0.9 min. Other authors attempted a statistical fitting of regular explosions using log-logistic and other theoretical distributions (e.g. Dominguez et al. (2016)). Thompson et al. (2002) reported 23 to 48 explosions in each 3-min-long time window recorded as tremor episodes during the 1999 eruption of Shishaldin Volcano, Alaska. These regular time-spaced episodes later transitioned to more irregular repose times where shorter and longer pauses coexisted.

Other examples with irregular repeat times have been recorded from eruptions on Hawaii and Etna. Pauses in the eruptive activity from 1989 to 2000 at Pu'u O'o (Kilauea volcano, Hawaii) were neither regular in duration nor in temporal spacing (Heliker and Mattox 2003). The frequency of 64 lava fountains in 2000 was neither repeating at regular intervals nor showed a systematic change (Alparone et al. 2003). In 2011, nine lava fountain episodes took place in irregular 5- to 10-day-long intervals (Carbone et al. 2015). In 2007, a perched lava channel within the Pu'u O'o flow field showed regular spattering every 40 to 100 min. Patrick et al. (2011) report two periods with fewer spattering events per day without commenting on likely reasons for the changes in duration of the events.

Systematic changes in repose time have been reported more rarely, e.g. in association with lava fountaining events on Etna (Moschella et al. 2018; Spampinato et al. 2015). Another example are tremor episodes due to rock column collapses during caldera formation, as happened in 2007 at Piton de la Fournaise. They became more closely spaced with time (Michon et al. 2007). The spacing pattern was in these cases unfortunately not investigated further.

Dominguez et al. (2016) developed an empirical relationship between median repose time and magma viscosity, based on eruptions at different volcanoes. However, whether changes in the magma viscosity systematically change the cyclic behaviour of one eruption remains an open question.

While regular, irregular or systematic changes within a pattern can take place, irregular patterns or systematic changes have not been investigated previously in detail. Triggers for these changes hence remain obscure. Here we investigate triggers that change the repeating tremor pattern of 7058 lava fountaining episodes that occurred in the Geldingadalir eruption on the Reykjanes Peninsula from 2 May to 14 June 2021.

The Reykjanes Peninsula, in Southwest Iceland, links the Western Volcanic Zone and the South Iceland Seismic Zone of Iceland to the offshore Reykjanes Ridge. The Reykjanes Peninsula features several northeast trending volcano-tectonic lineaments, also referred to as volcanic systems (e.g. Clifton and Kattenhorn (2006), Jakobsson et al. (1978), Sæmundsson and Sigurgeirsson (2013), Sæmundsson et al. (2020), Jakobsson et al. (2008), and Thordarson and Höskuldsson (2008)). They are from east to west: (i) Brennisteinsfjöll, (ii) Krýsuvík, (iii) Fagradalsfjall, (iv) Svartsengi and (v) Reykjanes. These volcano-tectonic lineaments are highly oblique to the plate boundary and plate movement (Jakobsson et al. 1978; Sæmundsson et al. 2020). All volcano-tectonic lineaments except Fagradalsfjall host a high-temperature geothermal system.

In the last 3.5 ka, the volcanic activity pattern was periodic, where 400- to 500-year-long eruption periods are separated by 800- to 1000-year-long periods of volcanic quiescence (Sæmundsson et al. 2020). The activity appears to migrate from the east to the west at a temporal spacing of 100 to 200 years (Sæmundsson et al. 2020). The last eruption period ended in 1240 CE (Jonsson 1983; Sæmundsson et al. 2020; Sigurgeirsson 1995). The Fagradalsfjall lineament features both Weichselian subglacial volcanic edifices and Holocene lava flow fields.

However, before 2021, it had not erupted in more than 6000 years (Sæmundsson and Sigurgeirsson 2013) and hence does not follow this episodic pattern of volcanism on the Peninsula. The 2021 eruption at Geldingadalir may be signalling the onset of a new eruption period on the Reykjanes Peninsula (Çubuk-Sabuncu et al. 2021; Flóvenz et al. 2022; Geirsson et al. 2021).

We study the tremor during episodes of lava fountaining and outflow of the 2021 Geldingadalir eruption ("Background and chronology of the Geldingadalir 2021 eruption" section) applying a STA/LTA triggering algorithm to data from a nearby seismometer ("Data acquisition and data analysis" section). We consider the growth of vent 5 ("Eruption behaviour and growth of the Crater-5 edifice" section) and the temporal tremor properties from March to mid-June ("Seismic spectral properties of the effusive tremor" section). We find systematic changes in the episode duration with time ("Gradual temporal changes in the fountaining duration and repose time" section), define different correlations behaviours of the episode duration and repose time ("Six periods in May and June with different fountaining pattern" section) and analyse the time window featuring both short and long episodes ("Coexisting short and long episodes in period 4" section). We discuss the details of one episode ("Magmatic processes and episodic venting of magma" section), reasons for the onset of the episodic fountaining ("Why did the eruption become episodic?" section), the decreasing and stable episode duration ("Change in tremor episode duration linked to an evolving shallow-conduit container" section), the gradual increase in the repose time ("Increasing repose time of fountaining episodes linked to magma accumulation in Crater" section), the coexistence of short and long episodes ("Coexistence of short and long tremor episodes" section) and the linearly increasing seismic amplitude ("Linear increase in seismic amplitude" section). We conclude that the fountaining pattern is affected by processes changing the boundary conditions and describe the evolving shallow-conduit container.

Background and chronology of the Geldingadalir 2021 eruption

After 781 years of quiescence (Jonsson 1983; Sæmundsson et al. 2020; Sigurgeirsson 1995), eruptive activity resumed on the Reykjanes Peninsula at approximately 20:30 UTC on 19 March 2021 (Barsotti et al. 2022). The eruption at Geldingadalir within the Mt. Fagradalsfjall complex was preceded by seismic unrest on the Reykjanes peninsula from December 2019, intrusions on the peninsula in 2020 (Çubuk-Sabuncu et al. 2021; Flóvenz et al. 2022; Geirsson et al. 2021) and seismic unrest in the Fagradalsfjall region from 24 February 2021 (Fischer et al. 2022; Sigmundsson et al. 2021). From 24 February, it was associated with the emplacement of a 9-km-long dyke between Fagradalsfjall and Keilir (Jonsdottir et al. 2021) (Fig. 1a).

On 19 March 2021, the eruption in Geldingadalir features 12 small vents each sitting on a 10- to 20-m-long northnortheast-trending en-echelon fracture, briefly defining a 180-m-long vent system. This initial activity becomes more and more localised and by 3:30 am (local time) on 20 March, there are 8 vents. By daybreak, it is confined to the two features that were later called vents 1a and 1b. These are the only vents active until 5 April 2021 (Fig. 1b and c) and supply the majority of the lava initially emplaced in Geldingadalir. The magma effusion is characterised by steady bubble-bursting to weakly fountaining activity accompanied by continuous lava outflow.

At 12:00 on 5 April, a new vent opens about 800 m northeast of the original vents in Geldingadalir (Fig. 1b). The activity on vent 2 begins in the same manner as for vent 1. In the following days, several new vents open between vents 1 and 2, with the last two (5 and 6) opening at 8:37 and 8:50 on 13 April (Fig. 1b and d). In the second half of April, these vents then become inactive and vents 1a, 1b and 5 were the only still active vents on 29 and possibly 30 April.

From the last day in April to 18 September, vent 5 is the only centre of activity. Vent 5 delivers lava to the flow field via internal (sealed) pathways along with episodic lava fountaining of variable intensity and periodicity (Figs. 1e to f and 2). Vent 5 features eruption episodes and repose times in the order of minutes in May to mid-July, in the order of hours in July and August and in the order of days in September.

The final eruption episode lasts from 11 to 18 September 2021 with one new lava outlet at the foothill of the wall of Crater-5. This outlet is northwest of the former vent 5. By the end of September 2021, the eruption has formed a volcanic cone rising about 120 m above the pre-eruption surface (Pedersen et al. 2022). The time-averaged magma discharge is steady at about $7\pm2.5\,m^3/s$ (DRE, range, 2 to $10\,m^3/s$, Bindeman et al. (2022). The total lava field covers about $5\,km^2$ and has an approximate DRE rock volume of $0.1\,km^3$ (Bindeman et al. 2022).

Data acquisition and data analysis

Instrument setup

We installed a Trillium Compact 120 s seismometer (Nanometrics) as station NUPH (9F seismic network) at the southeast corner of Núpshlídarháls (Eibl et al. 2022b).

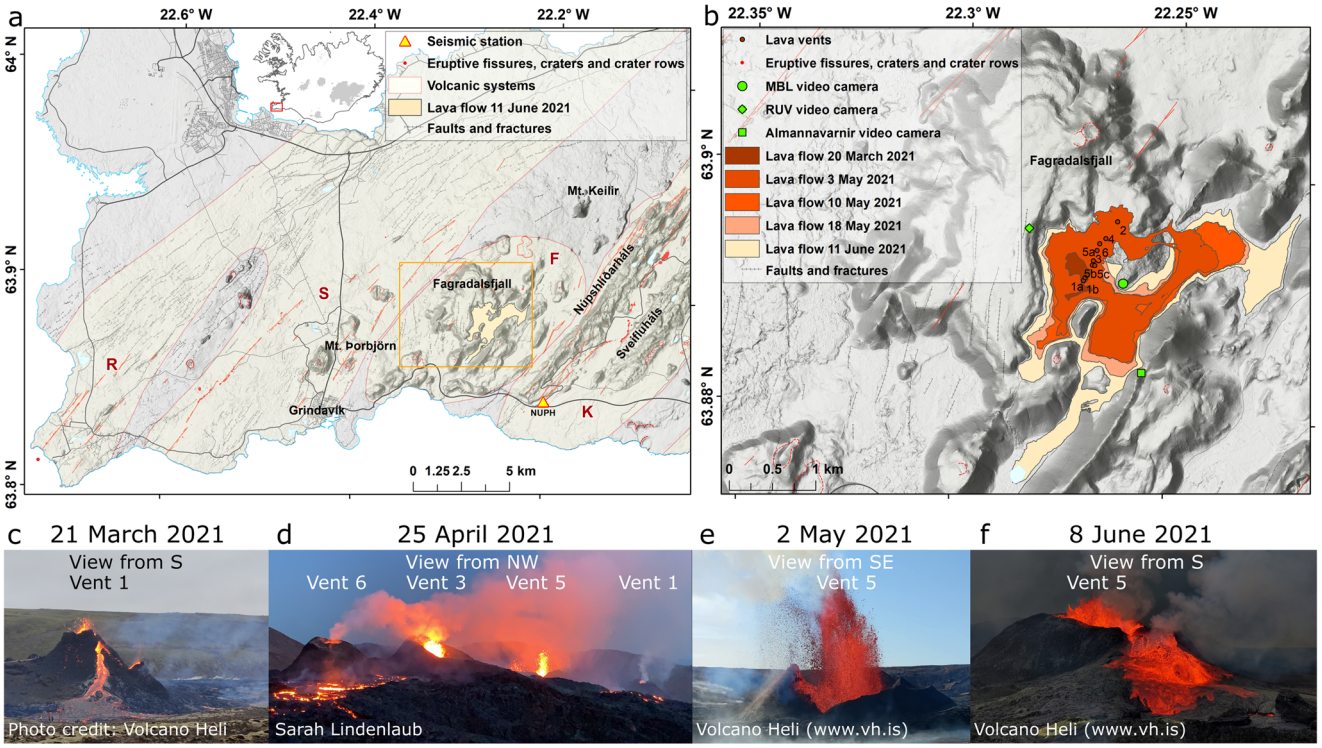

Fig. 1 Overview of the eruptive site and instrument location. (a) Overview and location of the Reykjanes Peninsula, Iceland. The volcanic systems are shaded light brown and marked with a bold letter, R-Reykjanes, S-Svartsengi, K-Krýsuvík (Sæmundsson and Sigurgeirsson 2013). The lava flow field (beige) and seismometer (triangle) are indicated. (b) Extent of the growing lava flow field and vent locations as derived in a collaboration of the National Land Survey of Iceland, the University of Iceland and the Icelandic Institute of Natural History (Bindeman et al. 2022; Halldórsson et al. 2022). The mbl, RUV and Almannavarnir camera location is marked. (c–f) Photos visualising the transition from steady lava outflow from vent 1 (c, 21 March), to steady lava outflow from multiple vents (d, 25 April, vents 2 and 4 not visible on photo), to lava fountaining (e, 2 May), to vigorous, splashing overflow at vent 5 (f, 8 June)

We recorded signals at 5.5 km southeast of the eruptive site in Geldingadalir, Iceland, from 12 March to 24 June 2021 (Fig. 1a). The instrument stood on a concrete base slab shielded from wind and rain using a bucket partly covered by rocks. Further common noise sources on the Reykjanes Peninsula are oceanic microseisms and surf noise on the shore. The instrument was powered using batteries from 12 March, solar panels from 24 March and a wind generator at 10-m distance from 6 April 2021. Data were sampled at 200 Hz, they were stored on a Datacube and regularly downloaded. We used a compass to align the instrument to geographic north.

Wind speeds higher than 5 m/s create strong noise on our sensor at frequencies above 1 Hz since it was not buried in the ground. Despite this noise in the tremor frequency band, the data quality is good enough to detect volcano-seismic signals such as tremor.

Seismic preprocessing

The seismic data are detrended, instrument response corrected to velocity, tapered and filtered between 1 and 4 Hz. We use the Pyrocko trace-viewer Snuffler to mark the start and end of the tremor episodes (Heimann et al. 2017). First, we use the built-in STA/LTA triggering algorithm (Trnkoczy 2012) on the sum of the 3 component seismic recordings of station NUPH. We use STA windows of 60 to 120 s and three times larger LTA windows in a moving time window. STA/LTA markers are then moved to the episode start and end. Finally, we manually review all markers and add, remove and time-correct them if necessary. We process the time window from 1 May to 14 June leading to 14116 markers (Eibl et al. 2022a).

We define the **tremor cycle duration** from the start of one episode to the start of the next tremor episode. The **tremor episode duration** is defined from the start to the end of one tremor episode. The **tremor repose time** is defined from the end of one tremor episode to the start of the next episode. Hence, the episode duration plus repose time equals the tremor cycle duration.

We calculate root mean square (RMS) seismic ground velocity in 30-s-long time windows and 50% overlap for the whole time period. We also calculate the mean RMS during a tremor episode and in the repose time.

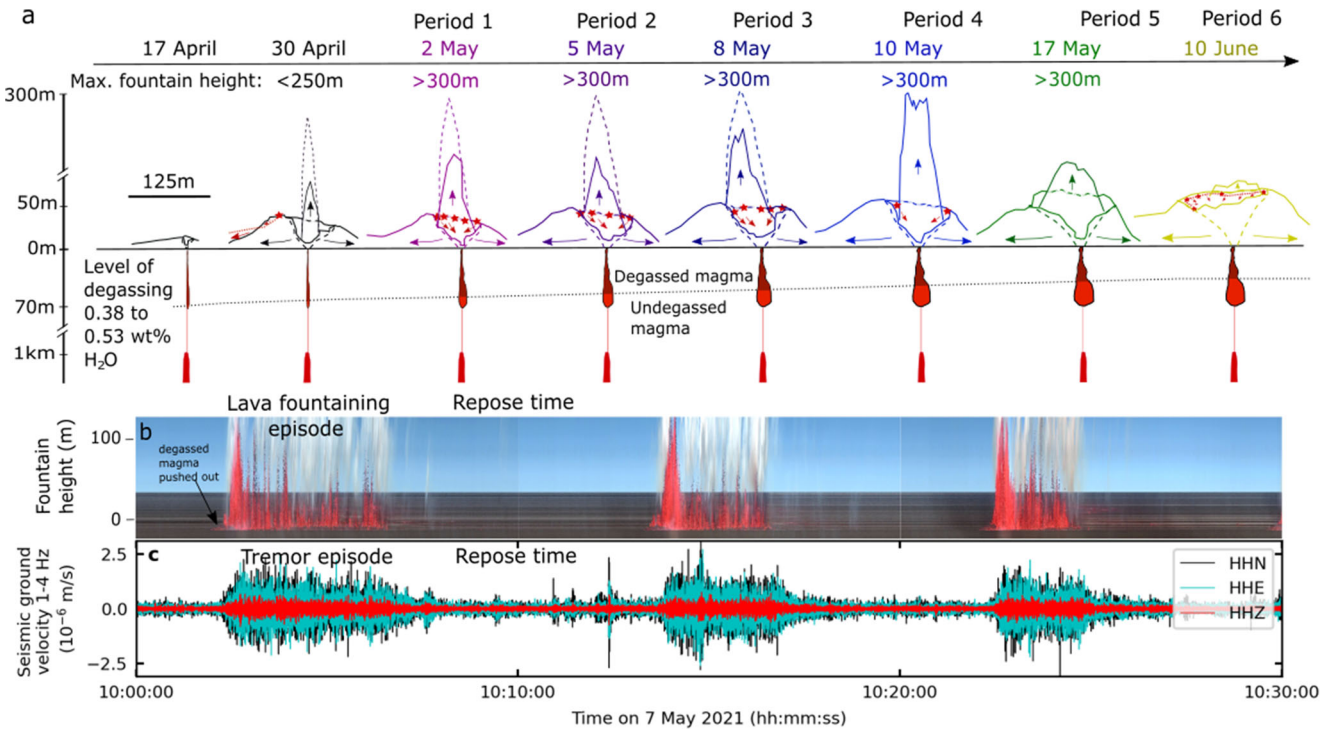

Fig. 2 Growth, fountaining and collapses of Crater-5 from 17 April to 10 June. (a) Coloured lines mark the crater shape at 14:00 on the respective date viewed from a camera from Almannavarnir on Langihryggur towards the northwest (Fig. 1b) and an exemplary (solid) and maximum (dashed) fountain height. Coloured arrows show lava outflow into the fountain or the lava flow field. Red stars mark collapses in the crater while dotted red lines show the fault plane and red arrows the collapse direction. The red and dark red colour indicates undegassed and degassed magma, respectively, accumulating in a shallow-conduit container evolving from 2 to 11 May. Water content and storage depth as in Bindeman et al. (2022). The red dike at 1-km depth feeds the eruption. The black dotted line indicates the depth at which degassing starts. (b) Kymograph highlighting the temporal changes in fountain height using a mbl camera (Fig. 1b) and (c) seismic ground velocity of 3 seismometer components

Video camera analysis

Morgunblað*i*ð (mbl.is) maintained a camera on a hill 390 m southeast of vent 5 (Fig. 1b) from 20:00 on 6 May to 11:00 on 18 May 2021. All Morgunblað*i*ð cameras are of type Hanwha techwin, models XNP-6120H and XNP-6040H. Due to the close proximity and low elevation, the camera was not affected by fog in this time period and recorded the eruptive activity reliably. We analyse data from this camera using a kymograph. This is an illustrative way of photo sequence analysis at geysers and volcanoes (Munoz-Saez et al. 2015; Witt and Walter 2017). To create a kymograph, we choose a vertical line from the ground through the active vent in all images, and plot the pixels' colour values of this line along a time axis. Video images are extracted at 1 frame per second. Using this time-space-plot, we identify the lava fountain occurrence, height and duration as recorded by the camera.

We extract the evolution of the vent and lava fountain height using a camera from Almannavarnir installed at the hill Langihryggur 1.3 km southeast of vent 5 (Fig. 1b). It recorded the whole time period from 1 May to 14 June. We extract single photos from the video using a VLC media player. We then open the photos in Inkscape to extract the vent shapes and exemplary fountain heights. To align all photos, we extract the shape of mount Fagradalsfjall that is visible in the background of all videos. The derived height is based on the people and cars in the foreground and mount Fagradalsfjall in the background. The uncertainty is in the range of $\pm$ 2 m.

We use a video camera from RUV that was installed on mount Fagradalsfjall northwest of vent 5 (Fig. 1b) to extract photos that show the collapse from 30 April to 2 May 2021.

Results

Eruption behaviour and growth of the Crater-5 edifice

In the first 4 days, vent 5 is surrounded by a few m-high ramparts which we call Crater-5 (Fig. 2a). Within 2 weeks, the crater grows quickly in height and dominates the other craters with a height of about 40 m on 30 April. A period of particularly rapid crater-wall growth at vent 5 occurs between 10 and 17 May, when the wall height increases by

15 m. The total height is about 60 m in mid-June. The walls of Crater-5 appear unstable until mid-May, but become more stable as they thicken with time and the surrounding lava flow field stabilises the crater. Overflow dominates in the south and northeast and thus these sides of the crater become less steep throughout May.

From 30 April to 18 May, the growing Crater-5 features frequent collapses from the walls on the western side, eastern side and northern side (Figs. 2a and 4f). From 15:45 on 30 April, cracks form in the Crater-5 walls resulting in a major outwards collapse of the southwestern flank towards the southwest (Figs. 2a and S1). This sliding was slow and persistent until 10:00 on 2 May. In the following days of May, several partial collapses occur daily. From 10 May and onwards, about one daily collapse happens from the crater rim. After 18 May, the only major collapse occurs at 4:18 on 10 June, when a circular fault forms along the crater rim and the inner part of the wall collapses into the crater. The collapse-related processes steadily widen the crater with time.

Through April, vent 5 is typified by a sustained and semi-steady activity of vesiculation (i.e. degassing), bubbling (i.e. outgassing) and intensifying fountaining, and lava outflow. For example, the fountain height reaches 250 m by 30 April, compared to heights of only a few meters in the early stages (13 to 15 April) of vent 5 activity. This pattern of vent 5 activity is driven by the gradual evolution of the top 1 km of the plumbing system. The effusion of magma semi-steadily becomes focused on the shallow conduit of vent 5, which culminates on 30 April when visible activity at vents 1a and 1b stops. In the early hours of 2 May, the pattern of activity described above was abruptly replaced by distinctly periodic activity, featuring eruption episodes with lava outpouring, outgassing and fountaining each punctuated by distinct lulls in activity.

An episode normally begins with a vesiculation-/degassing-driven, and escalating rise of the free magma surface in the crater. Shortly after the onset of the lava outpouring, visible bubbling (i.e. outgassing) at the free magma surface intensifies rapidly and leads to bursting of fast rising and expanding mega-bubbles (tens of meters in diameter), peaking in a run-a-way outgassing driving the vigorous and high fountains that typify the early stages of each episode in the period from 2 to 18 May when the maximum fountain heights exceed 300 m. When maximum fountain height is reached, outgassing had outpaced degassing and for the reminder of the episode, the activity becomes more pulsating. The fountaining vigor, intensity and height reduce in a semi-steady manner until the free magma surface drops abruptly and the episode comes to a sudden halt. At this stage, the bubble framework collapsed and outgassed lava residing in the crater retreats into the underlying shallow conduit compartment in a few minutes, leaving the crater empty during the repose time. From 18 May and onwards, the vigor of the activity in each episode was reduced significantly. The maximum fountain heights were much lower and the eruption behaviour transitioned to a fast-moving, vigorous, splashing lava over-flowing the crater rims in conjunction with effective outgassing and weak fountaining.

Seismic spectral properties of the effusive tremor

The volcanic tremor starts at 20:45 UTC on 19 March 2021. From March to 1 May, the eruptive tremor is continuous and characterised by energy below 3 Hz, strongest on the horizontal components (Fig. 3). The opening of new vents does not increase the tremor amplitude or spectral content recorded at NUPH. From 2 May, the tremor energy increases in all frequency bands, it broadens to 6 Hz and frequencies around 4 Hz increase in strength (Figs. 3a and f and S2). By 10 June, the tremor episode peak amplitude has linearly increased threefold (Figs. 3a to e and 4a). At 4:18 UTC on 10 June, this trend is disrupted when the tremor amplitude and energy in the spectrogram suddenly decrease (Fig. 3f and m).

Besides the long-term changes in the amplitude and frequency content of the tremor, the volcano enters a start and stop phase typified by episodic fountaining and periodic generation of associated surface flows from 2 May to 14 June. We record a tremor episode during lava fountaining or vigorous outflow (Fig. 2b and c) and no tremor when there is no visible activity in the vent (= tremor repose period). We speculate that the tremor source is stationary in this time period. From 14 to 25 June, continuous tremor with weak pulses reappears.

Gradual temporal changes in the fountaining duration and repose time

From 2 May to 14 June 2021, 7058 tremor episodes are recorded (Fig. 4). Episodes are detected on all three components of the seismometer (Fig. 4a). The wavefield is hence composed of SV- as well as SH-type waves while SH-type waves such as SH waves or Love waves clearly dominate over SV waves and Rayleigh waves. The tremor amplitude is similar on the north and east component throughout the time period (Fig. 4b). The seismic amplitude of the horizontal components is two times larger than the amplitude of the vertical component in the times of repose, and 3 to 4 times larger during episodes (Fig. 4b)

The RMS amplitude of the tremor episodes increases linearly with time (Fig. 4a). It is, however, affected by wind noise, for example from 25 to 31 May, from 3 to 4 June and from 8 to 9 June (compare Fig. 4a and d). To remove the wind noise, we subtract the seismic amplitude during the

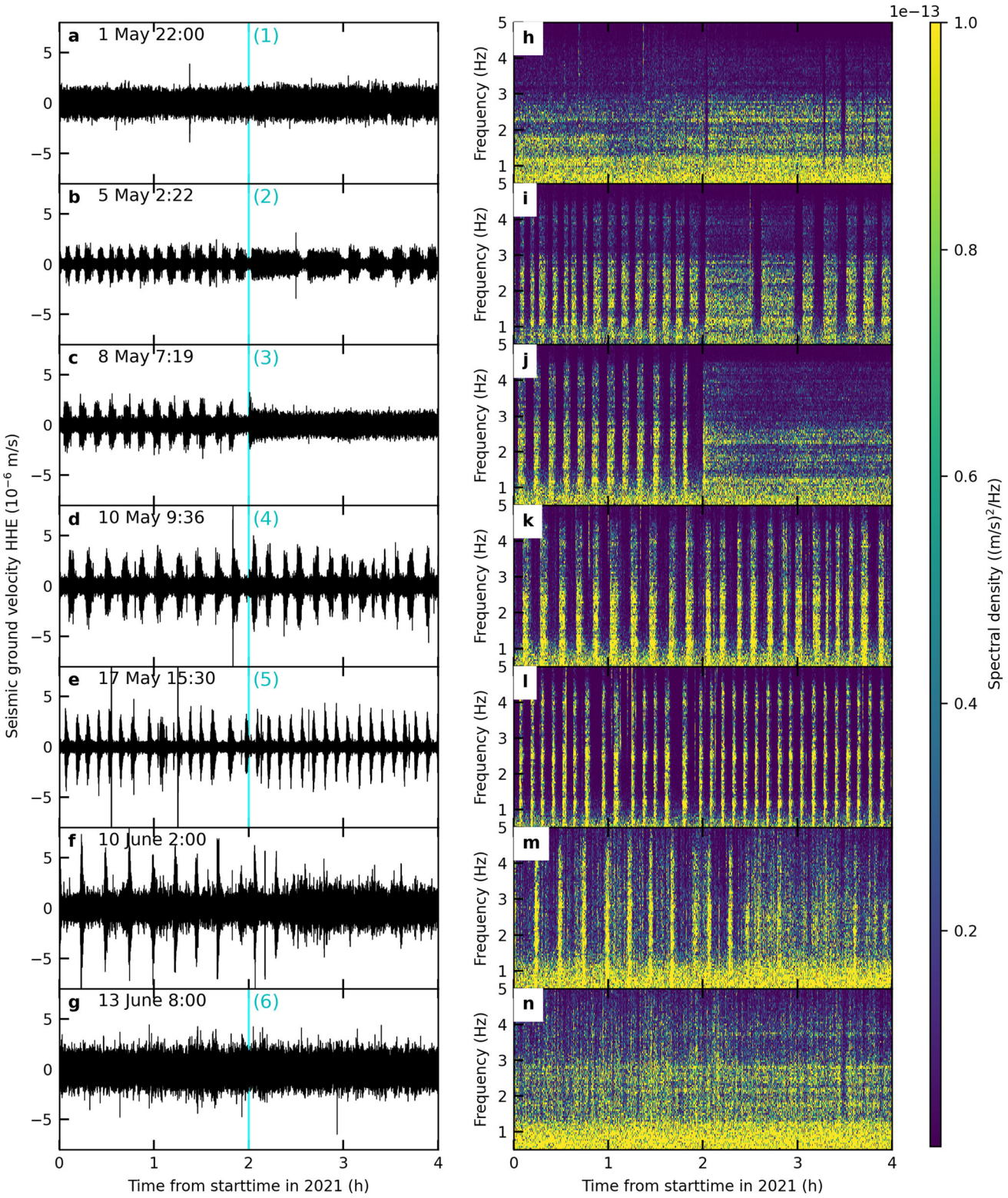

Fig. 3 The seismic amplitude increased and frequency content became broader between 1 May and 14 June 2021. (a–g) Four-hour-long seismograms of the east component of the seismometer. Date and time mark the start of the time window. The vertical cyan lines mark the changes in cyclic pattern and the onset of the six periods. (h–n) Four-hour-long spectrograms of subfigures (a)–(f) using a window length of 4096 samples and no overlap

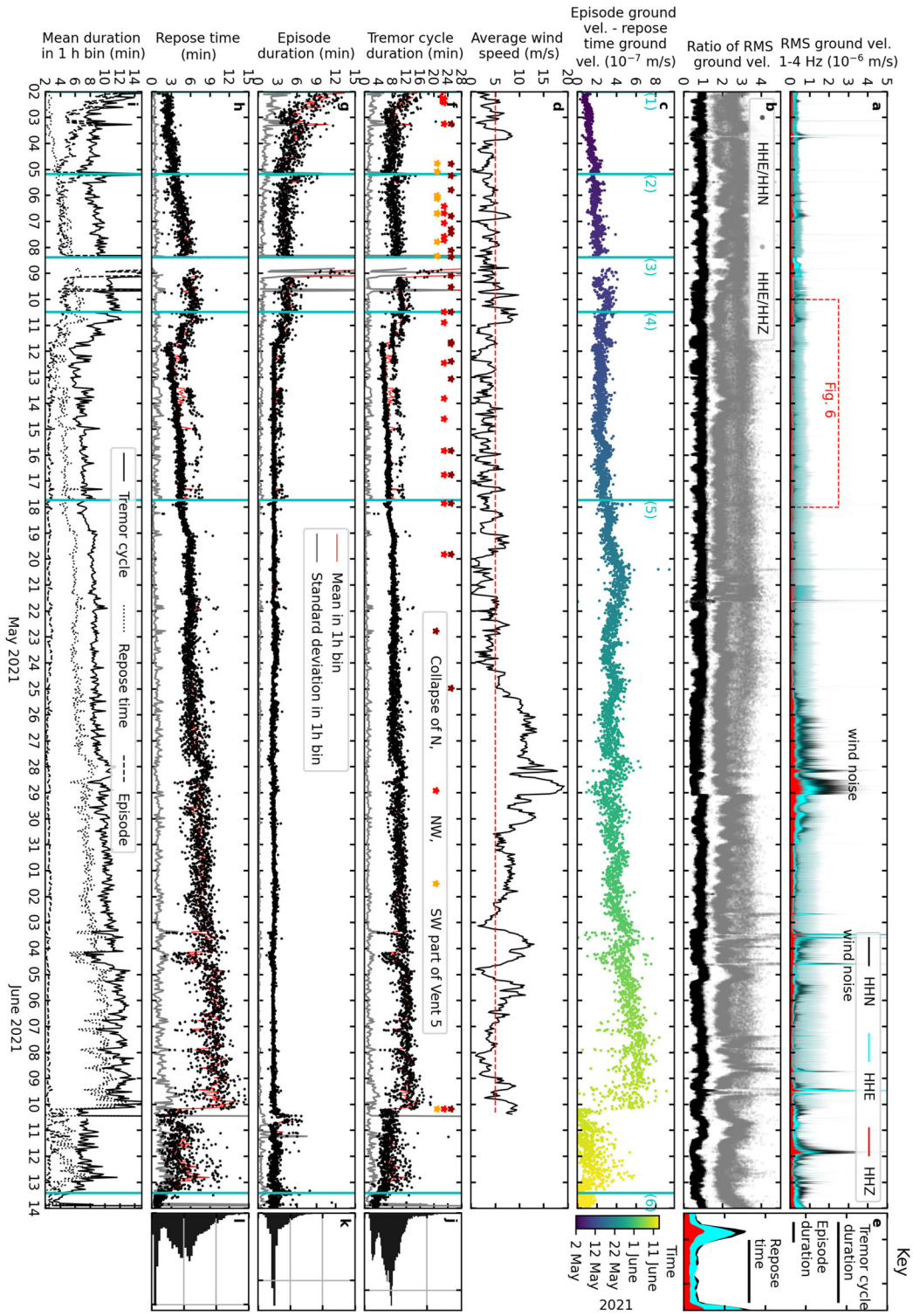

Fig. 4 The episode characteristics and repeating pattern change with time. (a) RMS of the seismic ground velocity on all three components filtered 1 to 4 Hz. (b) Ratio of RMS seismic ground velocities HHE/HHN (black) and HHE/HHZ (grey). (c) Episode ground velocity corrected for wind noise coloured according to time. Cyan vertical lines mark the periods 1 to 6. (d) Average wind speed measured by a weather station from IMO at Grindavík. The red horizontal line marks 5 m/s. (e) Key explaining cycle duration, episode duration and repose time from 12:12 to 12:23 on 1 June. (f) Tremor cycle duration (black dots), the mean (red line) and standard deviation (grey line) in a 1-h-long time window. Dark red, red and orange stars mark collapses of the northern, northwestern and southwestern part of the vent, respectively. (g) Same as subfigure (f) for episode duration and (h) repose time. (i) Mean duration as in subfigures (f)–(h). (j–l) Histograms of subfigures (f)–(h)

repose time from the seismic amplitude during the tremor episodes (Fig. 4c).

While the seismic amplitude increases linearly, the tremor cycle duration changes often and rapidly. We use these changes to define six periods (cyan vertical lines on Figs. 3 and 4 and Table 1). **Period 1**: The tremor cycle duration decreases from 13.1±3.5 min to 8±3 min on 3 May (Fig. 4f) and then remains stable until the early morning of 5 May. **Period 2**: The tremor cycle duration suddenly increases to 14±1 min at 4:22 on 5 May. Within 8 h, it decreases to 7.5±0.5 min and linearly increases to 9.7±0.4 min at 9:19 on 8 May. **Period 3**: Continuous tremor restarts at 9:19 and transitions to 17.2±0.8 min long episodes at 19:40. This tremor cycle duration shortens to 10.3±0.4 min on 9 May and linearly increases to 11.8±1 min on 10 May. **Period 4**: The cycle duration suddenly decreases to 8.2±0.3 min at 11:36 on 10 May and to 5.2±0.2 min at 16:00 on 11 May. The cycle duration then gradually increases to 7±0.2 min on 17 May at 17:30. Concurrently, cycles exist that are 3 min longer than the short cycles. **Period 5**: From 17 May at 17:30 to 10 June at 4:18, the duration increases from 7±0.2 to 15±0.4 min. At 4:18 on 10 June, the tremor amplitude and cycle duration suddenly decrease and the latter fluctuates between 5.4±1.5 and 10±3.4 min (Fig. 4f). **Period 6**: The tremor cycle duration decreases to a stable 3.5±0.5 min interval from 10:00 on 13 June.

The episode duration decreases exponentially from 11.4±3.2 min on 2 May to 5.5±2 min on 3 May (Fig. 4g). It then remains constant around 5.5 min until 10 May, although it is interrupted twice by longer episode durations from 4:22 to 12:00 on 5 May and continuous tremor from 9:19 to 19:40 and longer episodes thereafter to midnight on 8 May that mark the start of periods 2 and 3, respectively. In Period 4 the episode duration decreases abruptly at 11:36 on 10 May to 3.6±0.3 min and at 16:00 on 11 May to 2.4±0.2 min. In this period, 3.6-min-long episodes coexist with the dominant 2.4 min short ones. From 17 May in period 5, the episode duration is 2.5±0.1 min with standard deviations increasing to 0.5 min on 10 June. Tremor episodes become less visible after 10:00 on 13 June in period 6 when continuous tremor dominates again.

From the start of period 1 to the end of period 3, the tremor repose time increases linearly from 1.7±0.6 min to 6.4±0.5 min (Fig. 4h). In period 4, the repose time suddenly shortens to 4.6±0.7 min at 11:36 on 10 May and to 2.8±0.5 min at 16:00 on 11 May. From 11 May to 10 June, the repose time increases linearly to 12.5±2 min. In period 4, the short repose times alternate with 2-min longer repose times. In period 5, the longer repose times do not reappear. On 10 June, the repose time decreases suddenly and fluctuates between 3.5±1.8 and 7.0±3.1 min. In period 6, from 10:00 on 13 June, continuous tremor restarts with weak fluctuations in amplitude.

In general, the eruption features long episodes and short repose times in early May, and short episodes and long repose times in mid-June.

Six periods in May and June with different fountaining pattern

Here we examine the relationship between the tremor cycle duration, episode duration, repose time and seismic tremor amplitude in the above mentioned periods (Figs. 4i, 5 and S3 to S8).

In periods 1 to 3 (2 to 10 May), the cycle duration correlates with the episode duration. A longer tremor cycle at the start of periods 1, 2 and 3 is hence due to a longer tremor episode duration (Figs. 4f and 5a). However, with time the tremor cycle gradually lengthens, primarily due to the linearly increasing repose time. Hence, there is a weak correlation between the two parameters (Fig. S3c). The episode duration and repose time do not correlate in periods 1 to 3 (Fig. 5b).

In period 5 (17 May to 13 June), the cycle duration correlates well with the repose time (Fig. 5c) but not with the episode duration, which at this time is fairly constant (Fig. 5a and b). The collapse on 10 June does not affect this correlation. Period 6 starts on 13 June when cycle duration, episode duration and repose time all correlate (Figs. 5a and c and S8a and c).

In Fig. 5d–f, we compare the cycle duration, episode duration and repose time with the seismic amplitude corrected for wind noise. In periods 1–3 and 5, the mean episode amplitude correlates with the repose time, i.e. larger amplitude tremor episodes are followed by longer pauses to the next episode (Fig. 5e). Given the correlation between repose time and cycle duration in period 5, it follows that the seismic amplitude and tremor cycle duration correlate in period 5 (green to yellow points in Fig. 5d). No correlation exists between the amplitude and the episode duration for all periods (Fig. 5f) and the tremor cycle duration in periods 1 to 4 (blue points in Fig. 5d).

Coexisting short and long episodes in period 4

In period 4 (10 to 17 May), the cycle duration, the episode duration and the repose time decrease twice (Figs. 4f–h and 6b). As the tremor cycles become shorter from 10 towards 12 May, the number of cycles within a 2-h time interval doubles (Fig. 6c). After 13 May, the number of tremor cycles decreases, because the cycle duration increases.

Following the sudden decreases in cycle duration, short and longer tremor cycles coexist (Fig. 6a and b). Another interesting feature of individual cycles is that short repose

Table 1 Overview of tremor cycle duration, episode duration and repose times in all six periods

Unit: min	Period 1	Period 2	Period 3	Period 4	Period 5	Period 6
Start time	0:00 on 2 May	4:22 on 5 May	9:19 on 8 May	11:36 on 10 May	17:30 on 17 May	10:00 on 13 June
End time	4:22 on 5 May	9:19 on 8 May	11:36 on 10 May	17:30 on 17 May	10:00 on 13 June	
Cycle duration Trend	13.1±3.5 to 8±3 exponential	14±1 to 7.5±0.5 exponential 7.5±0.5 to 9.7±0.4 linear	17.2±0.8 to 10.3±0.4 exponential 10.3±0.4 to 11.8±1 linear	11.2±1 to 8.2±0.3 to 5.2±0.2 sudden drop 5.2±0.2 to 7±0.2 linear coexisting 3 min longer ones	7±0.2 to 15±0.4 linear from 10 June: 5.4±1.5 to 10±3.4	3.5±0.5 stable
Episode duration Trend	11.4±3.2 to 5.5±2 exponential 5.5±2 stable	14.9±10.2 to 5.5±2 exponential 5.5±2 stable	24.3±11.9 to 5.5±2 exponential 5.5±2 stable	4.8±2 to 3.6±0.3 to 2.4±0.2 sudden drop 2.4±0.2 stable coexisting 1 min longer ones	2.5±0.1 stable from 10 June: 2.5±0.5	2.5±0.5 stable
Repose time Trend	1.7±0.6 to 6.4±0.5 linear			6.4±0.5 to 4.6±0.7 to 2.8±0.5 sudden drop 2.8±0.5 to 4.5±0.3 linear coexisting 2 min longer ones	4.5±0.3 to 12.5±2 linear from 10 June: 3.5±1.8 to 7.0±3.1	1±0.4 stable

The values indicate the mean ± one standard deviation in 1-h time windows (Fig. 4i). Two values in one row denote a transition from the first to the second value while the trend in the line below describes the transition. If the trend changes during one period, this is noted with values and a trend in the third and fourth line of the respective box. Note that period 3 starts with continuous tremor from 9:19 to 19:40 and episodes of decreasing duration appear from 19:40

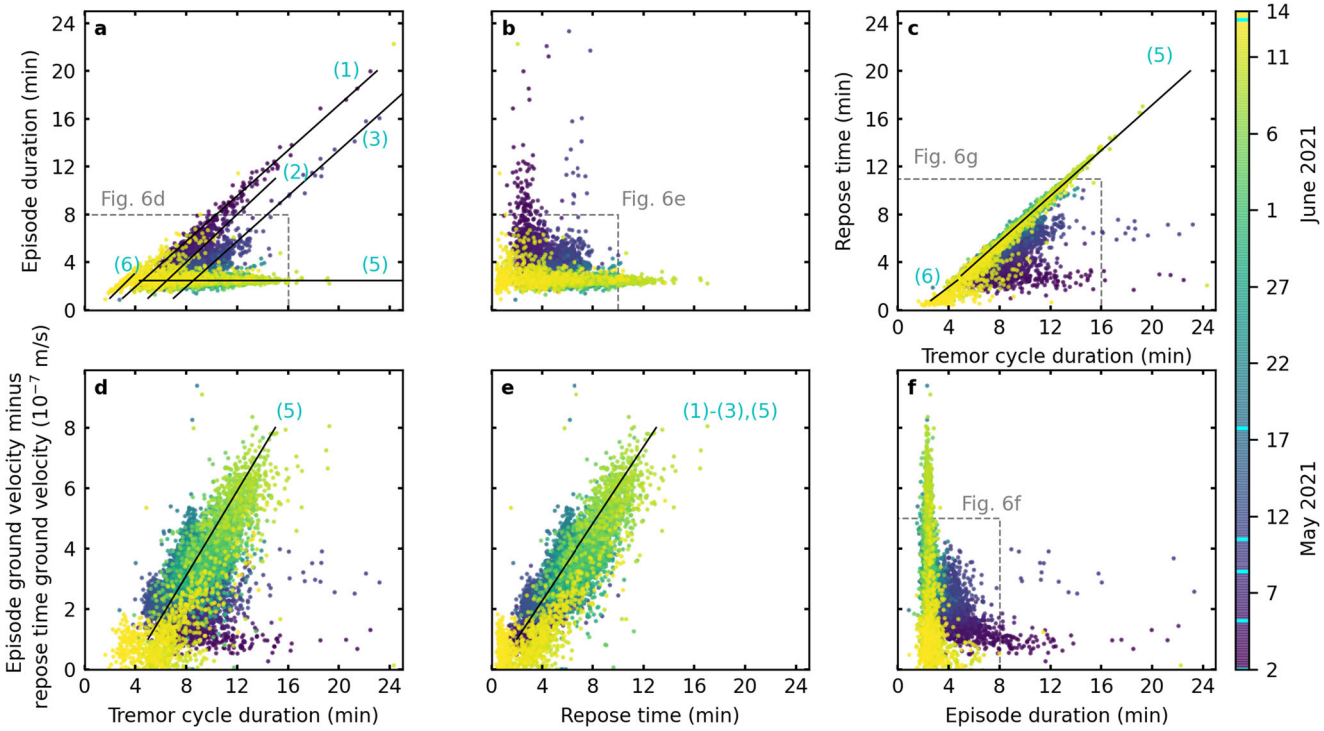

Fig. 5 Six periods exist from 2 May to 14 June with different correlation patterns. (a–b) Correlation of episode duration with (a) cycle duration and (b) repose time. Colours indicate the time. The labelled black lines highlight the correlation trends in periods 1 to 3, 5 and 6 in all subfigures. (c) Correlation of repose time and cycle duration. (d–f) Correlation of episode ground velocity corrected for wind noise and (d) cycle duration, (e) repose time and (f) episode duration. Points in period 4 lie in the grey dotted boxes (see also Fig. 6d–g)

times follow short episodes, and longer repose times follow longer episodes (Fig. 6a and e). The cycle duration, episode duration and repose time all correlate in period 4 (Fig. 6d, e and g). However, the seismic amplitude is not systematically affected by the episode duration (Fig. 6f) or the repose time.

Ten of the longer episodes consist of two amplitude peaks separated by an amplitude decrease of at least 50% of the maximum. In all other cases, we could not distinguish separate peaks (Fig. 6a). We refer to episodes with one and two clear peaks as single and double episodes, respectively (Fig. 6c). While the two peaks in a double episode have around 1-min temporal spacing, the following cycle persists 8 to 10 min. For single episodes, most cycles last 5 to 7 min (Fig. 6h and i). The double episodes appear between 11 and 16 May and are most dominant on 11 and 13 May (Fig. 6c).

We assess the temporal sequence of short and long tremor cycles using a Poincaré plot (Fig. 6h and i). Seventy-six percent of all episodes are short, while 24% of all episodes are long. The number of occurrences where a short episode follows a long one is identical to the number of occurrences of a long episode following a short one. Seventy-six percent of the short episodes are followed by a short one and 61% of the long episodes are followed by a long one. Forty-seven percent, 15%, 15% and 23% of the sequences are short-short, short-long, long-short and long-long, respectively. The sudden shortening and slow increase of the tremor cycle duration do not affect this sequence (Fig. 6i). Poincaré plots of all periods are shown in Fig. S9.

Discussion

Magmatic processes and episodic venting of magma

The magma erupted at Geldingadalir is basaltic, with a whole rock composition containing 47.1 to 49.8 wt% SiO_2 and 8.6 to 9.7 wt% MgO (the latter is most likely due to slight variations in abundance of olivine macrocrysts). Its initial water content ranges from 0.38 to 0.53 wt% (Bindeman et al. 2022). The estimated magma source depth ranges from 10 to 17 km or from a magma reservoir within the lower crust (Halldórsson et al. 2022). As basaltic magma rises from its storage reservoir, CO_2 begins to exsolve from the magma, and as the magma is under saturated in H_2O, its degassing is delayed until the magma is near the surface (Dixon and Stolper 1995; Dixon et al. 1995).

In case of the Geldingadalir eruption, water began to degas from the magma at 1.5- to 2.8-MPa pressure, equivalent to about 50- to 100-m depth (Newman and Lowenstern 2002). With initial magma discharge of ~4 m^3/s (DRE) and an erupting fissure length of 180 m

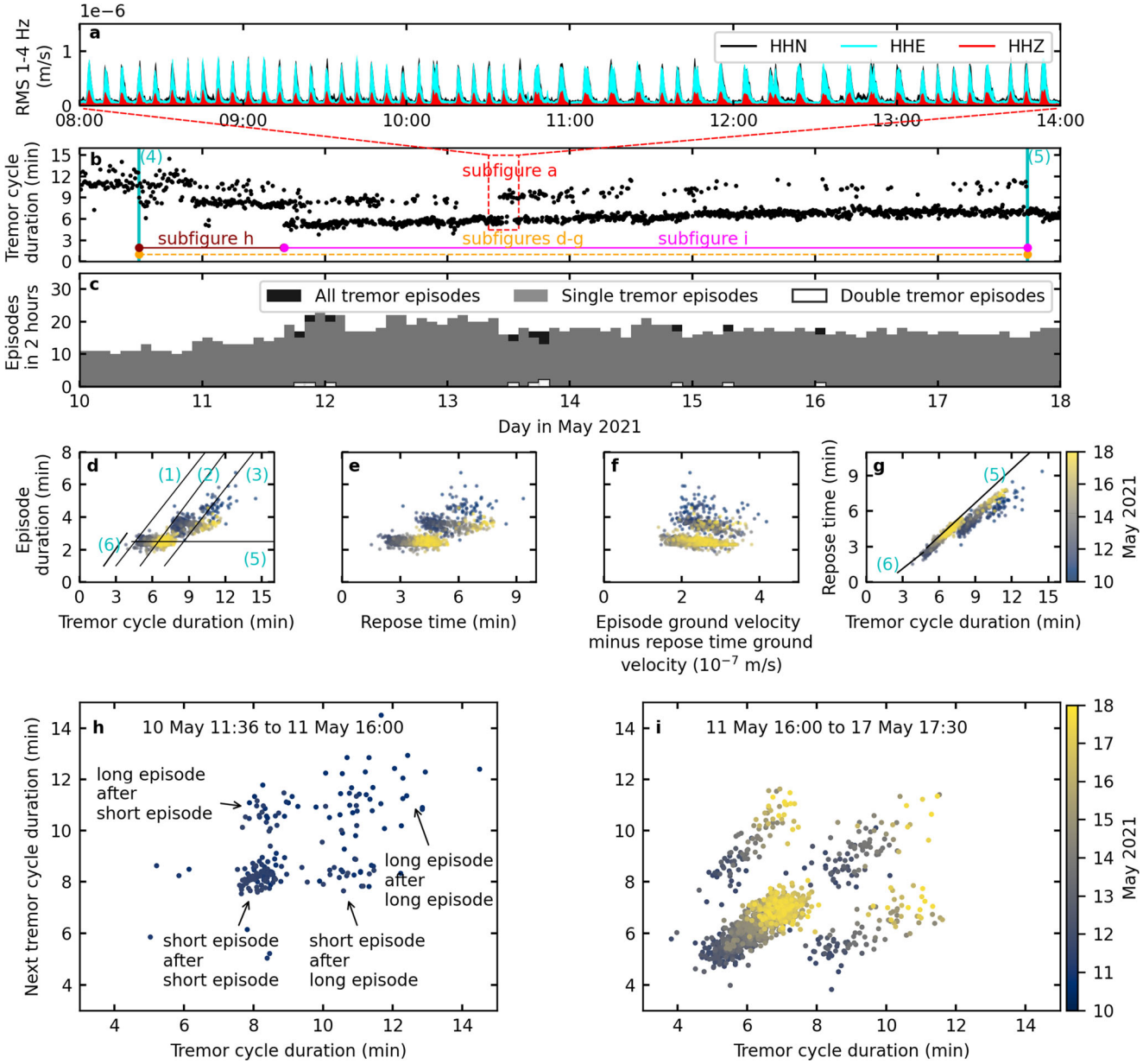

Fig. 6 Short and long episodes followed by short and long repose times, respectively, coexist in period 4 from 11:36 on 10 May to 17:30 on 18 May 2021. (a) Same as Fig. 4a zoomed in on 13 May from 8:00 to 14:00. (b) Dots and lines as Fig. 4f zoomed in from 10 to 18 May. The orange, horizontal line indicates the interval plotted in subfigures (d)–(g). The dark red and magenta lines mark the intervals in subfigures (h) and (i), respectively. (c) Number of tremor cycles per 2 h where all cycles (black), 1589 short cycles featuring one seismic peak (grey) and 10 long cycles featuring two seismic peaks (white) are highlighted. (d–f) Correlation of episode duration and (d) tremor cycle duration, (e) repose time and (f) episode ground velocity corrected for wind noise coloured according to time. (g) Correlation of repose time and tremor cycle duration. Black lines as in Fig. 5. (h–i) Poincaré plot where the tremor cycle duration is plotted vs. the next tremor cycle duration from (h) 11:36 on 10 May to 16:00 on 11 May and from (i) 16:00 on 11 May to 17:30 17 May

(e.g. Bindeman et al. (2022)) and an assumed fissure width of 1 m (Forslund and Gudmundsson 1991), the initial magma rise velocity is ~0.02 m/s in the Geldingadalir eruption. This rather slow magma ascent rate implies that the degassing driving each episode is most likely caused by continuous bubble nucleation within the above-mentioned depth interval (Houghton and Gonnermann 2008; Le Gall and Pichavant 2016).

In the period early to mid-April, the magma discharge increased from about 4 to 8 m^3/s (DRE) (e.g. Bindeman et al. (2022)) and consequently, new erupting vents open during the first half of April (Fig. 1). This sequence of

events was followed by their subsequent closure during the latter half of April. During this time, the eruption featured open-vent activity and steady outpouring of lava. Drone-derived observations of bubbling magma in the vents along with high vesicularity (> 70%) of erupted tephra clasts indicate that a two-phase flow (liquid and bubbles) had developed at the very top of the shallow conduit (Parfitt 2004). The decompression rate was about 500 Pa/s.

On 1 and 2 May, the activity became confined to a single vent, vent 5 and via our own on-site drone observations the magma issued from a 50–60-m-long and a 1-m-wide crack. At this time, as stated above, the magma discharge is 8 m^3/s DRE (Bindeman et al. 2022). Consequently, the magma ascent speed through the uppermost part of the conduit increased to 0.11–0.16 m/s, bringing the eruption into the Hawaiian eruption field (per classification of Parfitt et al. (1995)). This ascent rate indicates a minimum increase in decompression rate from 500 Pa/s in late April to 4000 Pa/s after 2 May. Degassing of H_2O and subsequent bubble nucleation and diffusion-driven bubble growth were the primary drivers of the eruptive activity at Geldingadalir (Sparks 1978). Higher decompression rates promote more intense lava fountaining (Head and Wilson 1987; Mangan et al. 2014; Parfitt 2004; Parfitt and Wilson 1994; 1995; 1999; Parfitt et al. 1995). Frequency and intensity of fountain episodes are driven by the amount of magma ready to degas at any one time (Mangan et al. 2014).

The free lava surface in the craters always fluctuated to a degree. However, it fluctuated most significantly after the activity became confined to vent 5 and the eruption behaviour was distinctly episodic — with the bubbly magma rising to the brim of the crater at peak activity in each eruption episode and dropping below the crater floor in the repose time. The lava that drained back into the shallow conduit at the end of each episode was outgassed (i.e. lost gas and bubbles). When in the underlying container, it sits on top of the magma column filling the plumbing system that continually replenishes the shallow conduit from below by fluxing of pristine and undegassed magma (Fig. 7). With increasing proportions of pristine magma, the free surface of the outgassed magma is pushed upwards and the system experiences decompression which initiates degassing and vesiculation. Because of the low melt viscosity, the bubbles nucleate easily, grow and rise rapidly, a process that lead to

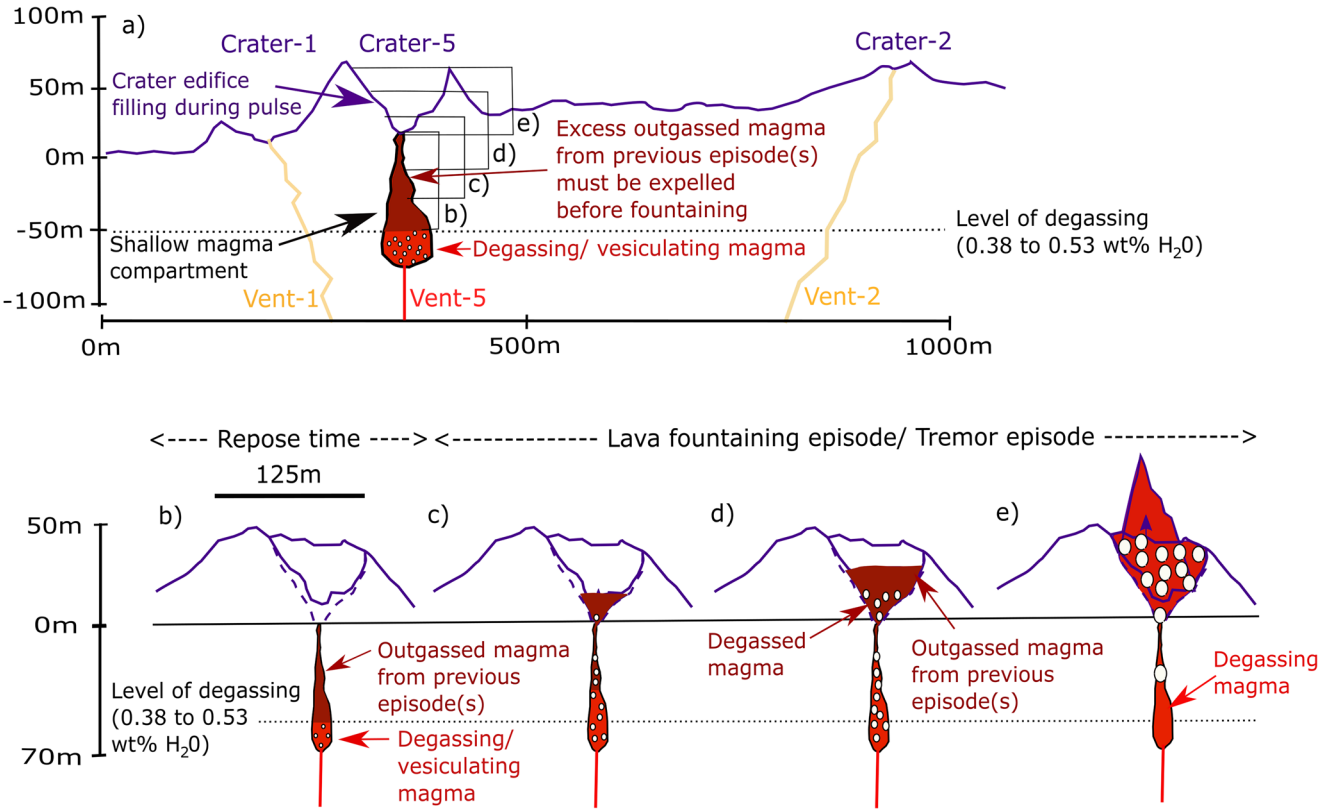

Fig. 7 Temporal evolution of lava effusion during a tremor episode. (a) Summarising the steps of lava effusion in the context of the other vents not effusing lava in May. (b) In the repose time, undegassed magma (red) accumulates beneath a cap of outgassed magma (dark red). (c–d) During the episode, the outgassed magma is pushed upwards into the crater by the undegassed magma. (e) During fountaining, the crater is full of hot and at this time degassing magma. Note that most of the volume is taken up by bubbles. Water content and storage depth as in Bindeman et al. (2022)

exponentially intensifying degassing from the newly arrived fresh magma (Fig. 7c) and formation of bubble strings as evident from development of (thermal) convection within the outgassed top of the magma column (Fig. 7d–e). Our on-site (i.e. drone based) observations show that the largest observed bubbles breaking the free surface within the crater had diameters of 20 to 50 m. This indicates bubble growth and coalescence from sub-micron size to tens of meters within the magma during a rise of 50 to 100 m. This process of escalating degassing pushes the degassed lava out of the crater. This further enhances the decompression rates, which results in run-away vesiculation, such that bubbles occupy the largest volume fraction of the magma filling the crater, eventually driving the lava fountaining activity.

At the onset of lava fountaining, the outgassing rates (= gas separated from the magma) start to exceed the rate of degassing (where gas moves into a bubble). This imbalance results in fountaining of waning intensity until this part of the system runs out of gas. Consequently, the fountaining comes to an abrupt halt, the magma volume in the crater collapses as the gas escapes and the outgassed magma drains rapidly into the underlying container.

Why did the eruption become episodic?

From the 5 to the end of April, up to six conduits feed magma to the surface. Each of these vents features semi-steady activity where magma degassing produces a steady bubble stream in the topmost part of the conduit resulting in perpetual bubbling and outgassing in the vents and continuous outflow of lava. As the vents shut down one by one from 17 to 30 April, the remaining active vents accommodate the additional flux and the lava fountain heights increase accordingly. This change is particularly well captured by the evolution at vent 5 from 23 to 30 April, which at that time is the main focus of the continuous activity: The fountain height and intensity grow exponentially based on the bubble nucleation theory. Around 01:00 of 2 May, the activity at vent 5 abruptly becomes episodic.

Around this time, eruption spectators reported hearing a deep, loud, thumping noise coming from the region between vents 1a/1b and vent 5, which are about 100 m apart. Activity at vents 1a/1b, which, as seen on timelapse videos, had been steadily dwindling for a few days, came to a halt at this time. In light of these on-site observations and the short distance between the two vents, it is reasonable to conclude that the separation between the shallow conduits of vents 1 and 5 collapses at this time on 2 May and forms the container that initiates and controls the rhythmic eruption behaviour. This magma container increases the magma volume available for near-simultaneous degassing (and outgassing) in the shallowest part of the conduit system, compared to the assumed 1-m-wide (Forslund and Gudmundsson 1991) dike-like conduits active in the first 6 weeks of the eruption.

It is likely that the major crater-rim collapse that took place on 30 April to 2 May aided the modulation to episodic behaviour (Fig. S1). When the crater-rim collapses came to a halt in the afternoon of 2 May, the tremor episode duration had shortened and stabilised at 8±3 min.

Hence, we propose that the abrupt shift to episodic eruption behaviour is due to the formation of the container at the top of the shallow conduit and its influence on degassing and outgassing processes. Other features, such as a steadily growing crater volume, periodic crater wall collapses and the retainment and recycling of older outgassed magma, are second-order features that produced punctuation-like (i.e. rim collapses) or gradual (rheology or geometrical) changes of the episodic rhythm. In the sections that follow, it is worthwhile to keep in mind that for the purpose of discussion, we assume that the magma supply rate from the source reservoir and the amount of undegassed magma reaching the shallow conduit compartment are effectively unchanged throughout May and until 14 June.

Change in tremor episode duration linked to an evolving shallow-conduit container

On 2 May, the tremor episode duration decreases exponentially (Fig. 4g). A similar pattern, but over a longer time span, was observed during the early stages of the 1983–2018 Pu'u 'O'o eruption in Hawai'i (Heliker and Mattox 2003), when the duration of the tremor episodes decreased exponentially from 12 to 0.5 days in the period from 1983 to 1986. Between 2 and 10 May, this exponential decrease in tremor episode duration repeats three times during the Geldingadalir eruption. From 11 to 17 May, the tremor episode duration is stable at about 2.5 min, but with periodic punctuations of tremor episodes of longer duration. After that, the longer episodes disappear altogether.

The pattern described above is interpreted as follows: The repeated periods of exponential decrease in tremor episode duration between 2 and 10 May are linked to periods were the volume of residual degassed magma in the shallow-conduit container increases. This is reflected in the transition from fast and often changing episode duration to stable episode duration (Fig. 4g). We interpret this to indicate a stepwise growth/enlargement of the shallow-conduit container until 11 May.

Furthermore, such growth may produce disturbances that lead to partial collapses of the crater rim; for example, at 8:03:52 on 8 May, when the southern rim partially collapses into the crater followed by a large collapse on the northern crater rim at 8:46:14 that lowered the rim by 10 to 15 m. Three powerful lava fountaining episodes

follow, including the most powerful one during the eruption reaching more than 300-m height. It is possible that these powerful episodes emptied the container to such a degree that it took a few hour to recover during the period of continuous tremor (period 3, Fig. 4a and f) and weak pulsing activity. No obvious other reason for the short-term change in behaviour could be found.

Stable episode duration as observed from 11 May suggests that a similar volume of magma degases in each episode, indicating that the shallow-conduit container reached a semi-steady form by the 17 May, when the punctuated longer duration episodes stop. Periodic enlargement of the shallow-conduit container implies rather abrupt increases in accumulated magma volumes and consequently, abundance of gas available for degassing, which may explain the brief periods of exponentially decreasing tremor episode duration.

On 10 and 11 May, the tremor cycle duration changes from 11.2±1 min, to 8.2±0.3 min and finally 5.2±0.2 min long cycles within a 29-h period (Fig. 6). Since short and long episodes coexist in this time period, this might indicate an underlying 3-min-long process in the shallow-conduit container that repeats two to four times. A partial collapse from the crater wall might reduce the threshold of the system for effusion, for example by releasing more of the outgassed magma from the vent. The variation in the fraction of outgassed magma retained in the vent may lead to tremor episodes of different durations in period 4. Other scenarios to explain the coexistence of short and long episodes such as a larger and a smaller shallow-conduit container seem unlikely due to the stable pattern of the episode duration and repose time.

Surprisingly, the system remains stable for several weeks so that subtle changes in the behaviour can be observed. This might be due to the slow and steady effusion at 5 to 15 m^3/s (Bindeman et al. 2022; Pedersen et al. 2022). In comparison, effusion rates up to 300 m^3/s were measured in the first few days of the Holuhraun eruption 2014/15 (Coppola et al. 2017; Eibl et al. 2017b) where continuous outflow dominated the eruptive style. If the effusion rate is higher, the system is pressurised and the geometry evolves faster to a stable status.

Interestingly, the repose time and the episode duration do not correlate. The only exception is period 4 when longer episodes are followed by a longer repose time. Similarly, Heliker and Mattox (2003) found that neither the pause before nor the pause after eruption correlated with the eruption duration, during the Pu'u 'Ō'ō-Kūpaianaha eruption in 1983 to 1986, Hawaii. We speculate that this indicates an evolving system where repose time and episode duration are affected by various factors.

Increasing repose time of fountaining episodes linked to magma accumulation in Crater

Throughout periods 1 to 3 and most of periods 4 and 5, the repose time increased linearly. Zobin (2013) reported a slowly increasing repose time between paroxysmal episodes on Etna over a few months, while tremor sources retreated to larger depths. At Piton de la Fournaise in 2007, the repose time of tremor episodes and collapses of the rock column systematically shortened (Michon et al. 2007). Alparone et al. (2003) observed a sudden increase in temporal spacing of paroxysms at Etna without clear drift in 2000. Moschella et al. (2018) reported temporal spacing of lava fountain episodes increasing from 5 to 20 days on Etna. However, the seismic amplitude did not increase systematically. Such systematic drift in behaviour can be due to geometrical changes in the shallow plumbing system, gas content or physical properties (Moschella et al. 2018). Spampinato et al. (2015) reported a linear increase in repose time of six fountaining episodes until it breaks down for the last four episodes in the sequence. They attribute this to faster magma transport and a more efficient degassing following stabilisation of the shallow conduit. In our case, such an interpretation might mean that the system keeps evolving until at least 14 June. However, based on the episode evolution, we suggest that it becomes meta-stable on 11 May and fully stable on 17 May.

The repose time may have increased due to growth of the shallow-conduit container at the top of the shallow conduit. If the size of the shallow-conduit container increases with time, more magma is needed to fill it and to trigger fountaining. A volume increase in the shallow-conduit container is supported by the observation that the continually growing crater was filled to the brim with bubbly lava during each episode, despite growing in volume with time. Since the repose time shortens on 10/ 11 May and 10 June, the shallow-conduit container must decrease in size, perhaps due to partial collapses from the crater rim. This could also explain shorter episodes after collapses in period 4. However, it is unlikely that the collapse material reaches the shallow-conduit container since the connection at the bottom of the crater is narrow.

Based on an analysis of 15 eruptions of different volcanoes, Dominguez et al. (2016) linked the median repose time of explosions within an eruption to the magma viscosity. Along these lines, the systematic increases in repose time that we report here might also relate to increases in the magma viscosity. Sudden decreases in repose time can then be caused by a viscosity decrease or be related to variations in the actual mass fraction of the degassed magma within the compartment or to variations in degree of cooling

experienced by the magma as it circulates at the interface with the atmosphere. However, the empirical relationship by Dominguez et al. (2016) was developed based on the median repose time during one eruption. Hence, fast changes in repose time within one eruption described here would require fast changes in magma viscosity.

Similar to the hypothesis on viscosity, we suggest that the repose time is linked to the degassed lava volume that remains in the crater or the shallow-conduit compartment at the end of individual episodes (Fig. 7). The crater height increases fast from 10 May (Fig. 2a). It also increases in width and finally closes on all sides increasing the lava volume steadily. More lava could accumulate in the crater during an episode and consequently the volume of residual degassed magma increased. To start a new episode, the increased volume of degassed lava needed to be cleared through and out of the crater, and thus may have increased the repose time from 10 May to 10 June (Fig. 4h). In this scenario, decreases in repose time may have been caused by collapse material that blocks the vent between the crater and the shallow-conduit container. If a collapse happens when lava resides in the crater, then it may disturb the pressure condition within the underlying degassing magma. This may start — depending on the exact state of system and size of the collapse — a lava fountaining episode. This hypothesis is challenged by the fact that after some episodes, the crater drains completely according to our drone observations. Further investigation is needed to assess the height of the base of the vent and volume of the crater.

Coexistence of short and long tremor episodes

The random sequence of short and longer episodes reminds us of Strokkur geyser in south Iceland. In the case of the Geldingadalir eruption, shorter episodes consist of 1 peak in seismic amplitude. Most of the longer episodes, however, consist of closely spaced peaks that merge into one and only for 10 episodes we detect two distinct separate peaks (Fig. 6a). We did not observe episodes containing three or more clear peaks. Similarly, the geyser Strokkur is characterised by single to sextuple eruptions, where sextuple eruptions are composed of six water fountains at an average temporal spacing of 16.1 s (Eibl et al. 2020). While 81% of the geyser eruptions are single eruptions, here we find that 76% of the episodes in phase 4 of the Geldingadalir eruption are short. We hence find a similarity of number and duration of single and double eruptions at Strokkur and the Geldingadalir eruption.

However, repose times for one eruption type at Strokkur are stable because there is no external or internal change in the system. Eibl et al. (2020) noted that the waiting time after eruptions linearly increases from single to sextuple eruptions. Similarly, longer episodes during the Geldingadalir eruption are followed by a longer repose time. While the geyser behaves repetitively, with no systematic change of eruption duration or frequency, the system at Geldingadalir evolved dynamically with time (Fig. 4f–h). While the geyser is a water-filled system driven by accumulating steam and superheated water, here the magma and the gas form a 2 phase system that is driven to eruption by the exsolution of H_2O and other volatiles such as S, CL and F from the magma. The underlying mechanisms are hence not comparable, but in period 4, it might be the best analog we have.

Linear increase in seismic amplitude

Assessing the seismic amplitude of one single tremor episode, it coincides in time with lava overflow in Crater-5 and subsequent fountaining (Fig. 2b and c). Tremor starts when the lava level in the crater begins to rise, in many cases leading to an overflow. The tremor peaks when the lava fountaining reaches the highest intensity and it stops when fountaining stops (Fig. 2b and c). Observations suggest that at the beginning of an episode degassed, viscous magma is pushed out of the crater, followed by less viscous and degassing magma towards the end of the episode. Similarly, a correlation between tremor episode and lava fountaining height was reported from Etna, Italy (Alparone et al. 2003; Falsaperla et al. 2005; La Spina et al. 2015; Tanguy and Patane 1984; Zobin 2013), Alaska (McNutt 1987) and Hawaii (Heliker and Mattox 2003).

At Geldingadalir from 2 May to 14 June, the peak seismic amplitude linearly increases and correlates with the repose time (Fig. 4c and h) but it never correlates with the episode duration. Similarly, Alparone et al. (2003) observed no correlation between the fountaining duration and the seismic amplitude on Etna. La Spina et al. (2015) reported a correlation between longer repose times and stronger tremor amplitude during fountaining on Etna. Based on chemical data, La Spina et al. (2015) suggest that on Etna the shallow-conduit container feeding, the eruption was gas overpressurised and that with time, more CO_2-rich gas reached the shallow-conduit container while the repose time increased. However, we have no data on the CO_2 flux to discuss this further. We suggest here that the system is stable from 11 May and that the inflow from magma is stable from May to mid-June. Based on the measured effusion rates, this is likely.

The increase in seismic amplitude might be linked to the increase in height and width of Crater-5 and the thickening crater walls. However, after 10 June, the seismic amplitude decreases after a major collapse on a circular fault inside

the crater. This further increases the uppermost crater width and reduces the wall thickness while the seismic amplitude decreases. The inner width of the crater decreases due to accumulation of debris in lower parts of the crater. We observe that the fountain height also increases alongside the increase in seismic amplitude in early May. However, in the second half of May, the lava fountains transition from 300-m high, episodic fountaining (Fig. 1e), to slow starting, swelling lava overflow, followed by few meter high fountains (Fig. 1f). While the fountain height decreases from 18 May, the seismic amplitude keeps increasing. Hence, the crater shape and fountain height cannot explain the observed amplitude pattern.

However, the transition to swelling, vigorous overflow of magma out of the crater with minor regular lava fountains (Fig. 1f) reflects the accumulation of degassed magma in the shallow-conduit container. During period 5, the degassing magma needs to go through still molten but degassed magma that affects its ascent and decompression rate, reflected in greatly reduced lava fountain height. This magma might see more friction in the uppermost magma column leading to increasing tremor amplitudes. However, during the collapse on 10 June, the lava properties and composition remain stable, while the tremor amplitude decreases threefold (Fig. 3f).

In a review of 24 eruptions of 18 volcanoes, McNutt and Nishimura (2008) found a proportionality between the square-root of the cross-sectional vent area and the tremor amplitude in reduced displacement. For the Geldingadalir eruption, this suggests that the collapse on 10 June reduces the vent dimensions, i.e. the cross-sectional area of the active part of the eruptive vent. This interpretation suggests that the increasing seismic amplitude from 2 May to 10 June is due to increasing active vent dimensions. This is likely, and collapses from the crater rim in early May do not significantly affect the tremor amplitude possibly due to their small volume.

We suggest that the seismic amplitude is not linked to the fountain height, crater height and width, or magma viscosity. Instead, we suggest that the dimensions of the eruptive vent at the bottom of the crater govern the seismic amplitude. Episodic fountaining, steady magma flow and heat mechanically erode and enlarge the vent and conduit. Note that Lamb et al. (2022) arrived at the same conclusion based on independent infrasound data. This enlargement reflects in larger seismic amplitudes as long as major collapses do not interfere with the vent dimensions. This enlarging vent might also explain the observed fountain height decrease from 17 May. However, it does not reduce the repose time since other factors contribute such as the degassed lava in the crater, the crater geometry and magma viscosity, and other parameters that are poorly constrained.

Conclusion

We analyse the volcanic tremor behaviour recorded during the Geldingadalir eruption, Southwest Iceland, from 19 March to 14 June 2021 using a seismometer. From 2 May, it features a tremor episode pattern that evolves with time. We define six different periods based on the tremor episode duration, tremor cycle duration and repose time pattern. The recorded tremor episodes coincide in time with episodes with up to 300-m-high lava fountains.

For our analysis, we note that for the purpose of the situations considered here, the magma composition, the magma supply rate, and the amount of undegassed magma reaching the shallow crust are effectively constant (Bindeman et al. 2022). In late April, the ascent velocity increases and Crater-5 partially collapses. In combination with an audible noise at the eruptive site on 2 May, we suggest that the preexisting shallow-conduit containers beneath Crater-1 and 5 merge. The formation influences the degassing and outgassing processes and starts the episodic lava fountaining phase.

Based on fast changes in the duration of lava fountaining episodes, we suggest that the system grows and evolves until 11 May. It then reaches a steady state featuring regular tremor episodes. The repose time gradually increases from 2 May to 10 June, which we link to the increasing viscosity and amount of degassed magma that remains at the bottom of the crater, after a fountaining episode stops. Both the tremor episode duration and repose time are affected by partial collapses of the crater. The collapsed material might block the vent that links the shallow-conduit container with the crater and disturb the pressure conditions of the system. Depending on the exact state of system and size of the collapse, this can start a lava fountaining episode. Based on our observations, we also suggest that the vent is mechanically eroded with time and its dimensions increase so that it causes increasing seismic amplitudes and decreasing fountain heights.

We conclude that subtle changes in a shallow conduit system or shallow-conduit container are important to determine the behaviour of an eruptive system and to explain the seismic, volcanic tremor. We notice that the upper 100 m of the dike near the surface are critical, as this is the bubble forming region. Internal and external changes in crater geometry and height, magma viscosity, vent dimension change the boundary conditions of the system and affect the fountaining pattern and frequency. This is possible during low-intensity eruptions with small effusion rates, but might also have implications for larger eruptions. The reported features can be further investigated in the context of modelling, detailed video camera data analysis, seismological tremor locations or effusion rate or degassing studies.

Supplementary Information The online version contains supplementary material available at https://doi.org/10.1007/s00445-022-01622-z.

Acknowledgements We thank Friðgeir Pétursson, Rögnvaldur Líndal Magnússon at ISOR and Daniel Vollmer at University of Potsdam for technical support in the field. We thank Sebastian Heimann for programming support, Sandeep for the kymograph images and Sarah Lindenlaub for providing photos. The meteorological data was supplied by the Icelandic Meteorological Office, retrieved 10 June 2020. We thank Undine Gnauck, Alea Joachim and Shaig Hamzaliyev for minor discussion and for creating and checking markers. We thank mbl as well as RUV and Almannavarnir for sharing their video camera data with us for research purposes.

Author contribution Eva Eibl initiated the study conception and design. Data collection was performed and supported by Gylfi Páll Hersir, Egill Á. Gudnason, Thorbjörg Ágústsdóttir and Eva Eibl. Data analysis was performed by Eva Eibl, Thor Thordarson and Ármann Höskuldsson. The first manuscript draft was written by Eva Eibl and all authors commented on previous versions of the manuscript. All authors read and approved the final manuscript.

Funding Open Access funding enabled and organized by Projekt DEAL.

Data availability Seismic data from station NUPH are available via GEOFON (Eibl et al. 2022b). The list of tremor episode start and end times is available at GFZ Data Services (Eibl et al. 2022a).

Declarations

Competing interests The authors declare no competing interests.

References

Alparone S, Andronico D, Lodato L, Sgroi T (2003) Relationship between tremor and volcanic activity during the Southeast Crater eruption on Mount Etna in early 2000. J Geophys Res Solid Earth 108(B5):1–13

Andronico D, Cannata A, Di Grazia G, Ferrari F (2021) The 1986–2021 paroxysmal episodes at the summit craters of Mt. Etna: insights into volcano dynamics and hazard. Earth Sci Rev 220:103686

Azzalini A, Bowman AW (1990) A look at some geyser data from Old Faithful geyser. Appl Statist 39(3):357–365

Barsotti S, Parks MM, Pfeffer MA, Óladóttir BA, Barnie T, Titos MM, Jónsdóttir K., Pedersen GB, Hjartardóttir ÁR, Stefansdóttir G, Johannsson T, Arason Ó, Gudmundsson MT, Oddsson B, Þrastarson RH, Ófeigsson BG, Vogfjörd K, Geirsson H, Hjörvar T, von Löwis S, Pedersen GN, Sigurðsson EM (2022) The eruption in Fagradalsfjall (2021 Iceland): how the operational monitoring and the volcanic hazard assessment contributed to its safe access. Research Square; 2022. https://doi.org/10.21203/rs.3.rs-1453832/v1

Bindeman I, Deegan F, Troll V, Thordarson T, Höskuldsson A, Moreland W, Zorn E, Shevchenko A, Walter T (2022) Diverse mantle components with invariant oxygen isotopes in the 2021 Fagradalsfjall eruption Iceland. Nature Communications

Cannata A, Catania A, Alparone S, Gresta S (2008) Volcanic tremor at Mt. Etna: inferences on magma dynamics during effusive and explosive activity. J Volcanol Geotherm Res 178(1):19–31

Carbone D, Zuccarello L, Messina A, Scollo S, Rymer H (2015) Balancing bulk gas accumulation and gas output before and during lava fountaining episodes at Mt. Etna. Sci Rep 5

Clifton A, Kattenhorn S (2006) Structural architecture of a highly oblique divergent plate boundary segment. Tectonophysics 419:27–40

Coppola D, Ripepe M, Laiolo M, Cigolini C (2017) Modelling satellite-derived magma discharge to explain caldera collapse. Geology 45(6):523–526

Çubuk-Sabuncu Y, Jónsdóttir K, Caudron C, Lecocq T, Parks MM, Geirsson H, Mordret A (2021) Temporal seismic velocity changes during the 2020 rapid inflation at Mt. Þorbjörn-Svartsengi, Iceland, using seismic ambient noise. Geophys Res Lett 48(11):1–10

Dixon J, Stolper E, Holloway J (1995) An experimental study of water and carbon dioxide solubilities in mid ocean ridge basaltic liquids. Part I: Calibration and solubility models. J Petrol 36:1607–1631

Dixon JE, Stolper EM (1995) An experimental study of water and carbon dioxide solubilities in mid-ocean ridge basaltic liquids. Part II: Applications to degassing. J Petrol 36:1633–1646

Dominguez L, Pioli L, Bonadonna C, Connor CB, Andronico D, Harris AJ, Ripepe M (2016) Quantifying unsteadiness and dynamics of pulsatory volcanic activity. Earth Planet Sci Lett 444:160–168

Eibl EP, Bean CJ, Vogfjörd KS, Ying Y, Lokmer I, Möllhoff M, O'Brien GS, Pálsson F (2017a) Tremor-rich shallow dyke formation followed by silent magma flow at Bárdarbunga in Iceland. Nat Geosci 10(4):299–304

Eibl EPS, Bean CJ, Jónsdóttir I, Höskuldsson A, Thordarson T, Coppola D, Witt T, Walter TR (2017b) Multiple coincident eruptive seismic tremor sources during the 2014-2015 eruption at Holuhraun, Iceland. J Geophys Res Solid Earth 122(4):2972–2987

Eibl EPS, Gnauck U, Hamzaliyev S, Hersir GP, Gudnasson E, Pétursson F (2022a) Catalog of start and end times of lava fountaining episodes from 2 May to 14 June 2021 during the Fagradalsfjall eruption

Eibl EPS, Hainzl S, Vesely NIK, Walter TR, Jousset P, Hersir GP, Dahm T (2020) Eruption interval monitoring at Strokkur Geyser, Iceland. Geophysical Research Letters

Eibl EPS, Hersir GP, Gudnason EÁ, Pétursson F (2022b) 2-year seismological experiment near Fagradalsfjall, Reykjanes peninsula in 2021/22. GFZ Data Services. Other/Seismic Network

Falsaperla S, Alparone S, D'Amico S, Grazia G, Ferrari F, Langer H, Sgroi T, Spampinato S (2005) Volcanic tremor at Mt. Etna, Italy, preceding and accompanying the eruption of July - August, 2001. Pure Appl Geophys 162(11):2111–2132

Fischer T, Hrubcová P, Salama A, Doubravová J, Horálek J, Ágústsdóttir T, Gudnason EÁ, Hersir GP (2022) Swarm seismicity illuminates stress transfer prior to the 2021 Fagradalsfjall eruption in Iceland. Earth and Planetary Science Letters

Flóvenz ÓG, Wang R, Hersir GP, Dahm T, Hainzl S, Vassileva M, Drouin V, Heimann S, Isken M, Gudnason EÁ, Ágústsson K, Ágústsdóttir T, Horalek J, Motagh M, Walter T, Rivalta E, Jousset P, Krawczyk C, Milkereit C (2022) Cyclical geothermal unrest as a precursor to Iceland's 2021 Fagradalsfjall eruption. Nat Geosci 15:397–404

Forslund T, Gudmundsson A (1991) Crustal spreading due to dikes and faults in southwest Iceland. J Struct Geol 13(4):443–457

Geirsson H, Parks M, Vogfjörd K, Einarsson P, Sigmundsson F, Jónsdóttir K, Drouin V, Ófeigsson BG, Hreinsdóttir S, Ducrocq C (2021) The 2020 volcano-tectonic unrest at Reykjanes Peninsula Iceland: stress triggering and reactivation of several volcanic systems. In: EGU general assembly conference abstracts

Gudmundsson MT, Jónsdóttir K, Hooper A, Holohan EP, Halldórsson SA, Ófeigsson BG, Cesca S, Vogfjörd KS, Sigmundsson F, Högnadóttir T, Einarsson P, Sigmarsson O, Jarosch AH, Jónasson K, Magnússon E, Hreinsdóttir S, Bagnardi M, Parks MM, Hjörleifsdóttir V, Pálsson F, Walter TR, Schöpfer MPJ, Heimann S, Reynolds HI, Dumont S, Bali E, Gudfinnsson GH, Dahm T, Roberts MJ, Hensch M, Belart JMC, Spaans K, Jakobsson S, Gudmundsson GB, Fridriksdóttir HM, Drouin V, Dürig T., Adalgeirsdóttir G, Riishuus MS, Pedersen GBM, Van Boeckel T, Oddsson B, Pfeffer MA, Barsotti S, Bergsson B, Donovan A, Burton MR, Aiuppa A (2016) Gradual caldera collapse at Bárdarbunga volcano, Iceland, regulated by lateral magma outflow. Science 353(6296):262

Halldórsson SA, Marshall EW, Caracciolo A, Matthews S, Bali E, Rasmussen MB, Ranta E, Robin JG, Guðfinnsson GH, Sigmarsson O, Maclennan J, Jackson MG, Whitehouse MJ, Jeon H, van der Meer QH, Mibei GK, Kalliokoski MH, Repczynska MM, Rúnarsdóttir RH, Sigurðsson G, Pfeffer MA, Scott SW, Kjartansdóttir R, Kleine BI, Oppenheimer C, Aiuppa A, Ilyinskaya E, Bitetto M, Giudice G, Stefánsson A (2022) Rapid source shifting of a deep magmatic system revealed by the Fagradalsfjall eruption, Iceland. Nature

Head JW, Wilson L (1987) Lava fountain heights at Pu'u 'O'o, Kilauea, Hawaii: indicators of amount and variations of exsolved magma volatiles. J Geophys Res Solid Earth 92(B13):13715–13719

Heimann S, Kriegerowski M, Isken M, Cesca S, Daout S, Grigoli F, Juretzek C, Megies T, Nooshiri N, Steinberg A, Sudhaus H, Vasyura-Bathke H, Willey T, Dahm T (2017) Pyrocko - an open-source seismology toolbox and library. V 0.3. Technical report, GFZ

Heliker C, Mattox TN (2003) The first two decades of the Pu'u 'Ō'ō-Kūpaianaha eruption: chronology and selected bibliography. U.S. Geological Survey Professional Paper

Houghton BF, Gonnermann HM (2008) Basaltic explosive volcanism: constraints from deposits and models. Chemie der Erde - Geochem 68(2):117–140

Jakobsson S, Jónasson K, Sigurdsson L (2008) The three igneous rock series of Iceland. Jökull 58:117–138

Jakobsson S, Jónsson J, Shido F (1978) Petrology of the Western Reykjanes Peninsula, Iceland. J Petrol 19(4):669–705

Jonsdottir K, Sabuncu YC, Geirsson H, Klaasen S, Caudron C, Lecocq T, Barsotti S, Barnie T, Sigmundsson F, Oddsson B et al (2021) Seismic monitoring of the 2021 Fagradalsfjall eruption, SW Iceland. In: AGU Fall Meeting 2021. AGU

Jonsson J (1983) Eldgos á sögulegum tíma á Reykjanesi (in Icelandic). Náttúrufræðingurinn 52:127–174

Kumagai H, Ohminato T, Nakano M, Ooi M, Kubo A, Inoue H, Oikawa J (2001) Very-long-period seismic signals and caldera formation at Miyake Island, Japan. Science 293(5530):687–690

La Spina A., Burton M, Allard P, Alparone S, Muré F (2015) Open-path FTIR spectroscopy of magma degassing processes during eight lava fountains on Mount Etna. Earth Planet Sci Lett 413:123–134

Lamb OD, Gestrich JE, Barnie TD, Jónsdóttir K, Ducrocq C, Shore MJ, Lees JM, Lee SJ (2022) Acoustic observations of lava fountain activity during the 2021 Fagradalsfjall eruption, Iceland 1 Introduction. Bull Volcanol 84(96)

Langer H, Falsaperla S, Masotti M, Campanini R, Spampinato S, Messina A (2009) Synopsis of supervised and unsupervised pattern classification techniques applied to volcanic tremor data at Mt Etna, Italy. Geophys J Int 178(2):1132–1144

Le Gall N, Pichavant M (2016) Homogeneous bubble nucleation in H2O- and H2O-CO2-bearing basaltic melts: results of high temperature decompression experiments. J Volcanol Geotherm Res 327:604–621

Mangan M, Cashman K, Swanson D (2014) The dynamics of Hawaiian-style eruptions: a century of study. In: Poland M, Takahashi T, Landowski C (eds) Characteristics of Hawaiian volcanoes. USGS professional paper 1801

McNutt SR (1987) Volcanic tremor at Pavlof Volcano, Alaska, October 1973-April 1986. Pure Appl Geophys PAGEOPH 125(6):1051–1077

McNutt SR, Nishimura T (2008) Volcanic tremor during eruptions: temporal characteristics, scaling and constraints on conduit size and processes. J Volcanol Geotherm Res 178(1):10–18

Michon L, Staudacher T, Ferrazzini V, Bachèlery P, Marti J (2007) April 2007 collapse of Piton de la Fournaise: a new example of caldera formation. Geophys Res Lett 34(21)

Moschella S, Cannata A, Di Grazia G, Gresta S (2018) Insights into lava fountain eruptions at MT. Etna by improved source location of the volcanic tremor. Ann Geophys 61(4)

Munoz-Saez C, Manga M, Hurwitz S, Rudolph ML, Namiki A, Wang CY (2015) Dynamics within geyser conduits, and sensitivity to environmental perturbations: insights from a periodic geyser in the El Tatio geyser field, Atacama Desert, Chile. J Volcanol Geotherm Res 292:41–55

Newman S, Lowenstern JB (2002) VolatileCalc: a silicate melt–H2O–CO2 solution model written in Visual Basic for excel. Comput Geosci 28(5):597–604

Parfitt E (2004) A discussion of the machanisms of explosive basaltic eruptions. J Volcanol Geotherm Res 134:77–107

Parfitt E, Wilson L (1994) Pu' u 'O'o eruption of Kilauea volcano, Hawaii: a study of dike geometry and eruption mechanisms for a long-lived eruption. J Volcanol Geotherm Res 59:179–205

Parfitt E, Wilson L (1995) Explosive volcanic eruptions IX. The transition between Hawaiian-style lava fountaining and Strombolian explosive activity. Geophys J Int 121:226–232

Parfitt E, Wilson L (1999) A Plinian treatment of fallout from Hawaiian lava fountains. J Volcanol Geotherm Res 88:67–75

Parfitt E, Wilson L, Neal C (1995) Factors influencing the height of Hawaiian lava fountains: implications for the use of fountain height as an indicator of magma gas content. Bull Volcanol 57:440–450

Patrick MR, Orr T, Wilson D, Dow D, Freeman R (2011) Cyclic spattering, seismic tremor, and surface fluctuation within a perched lava channel, Kīlauea Volcano. Bull Volcanol 73(6):639–653

Pedersen GBM, Belart JMC, Óskarsson BV, Gudmundsson MT, Gies N, Högnadóttir T, Hjartardóttir ÁR, Pinel V, Berthier E, Dürig T, Reynolds HI, Hamilton CW, Valsson G, Einarsson P, Ben-Yehosua D, Gunnarsson D, Oddsson B (2022) Volume,

effusion rate, and lava transport during the 2021 Fagradalsfjall eruption: results from near real-time photogrammetric monitoring. Geophysical Research Letters

Privitera E, Sgroi T, Gresta S (2003) Statistical analysis of intermittent volcanic tremor associated with the September 1989 summit explosive eruptions at Mount Etna, Sicily. J Volcanol Geotherm Res 120:235–247

Sæmundsson K, Sigurgeirsson MÁ (2013) The Reykjanes Peninsula. In: Sólnes J, Sigmundsson F, Bessason B (eds) Natural hazards in Iceland, volcanic eruptions and earthquakes (in Icelandic), pp 379–401. Viðlagatrygging Íslands/Háskólaútgáfan, Reykjavík

Sæmundsson K, Sigurgeirsson MÁ, Friðleifsson GǴ (2020) Geology and structure of the Reykjanes volcanic system, Iceland. J Volcanol Geotherm Res 391:106501

Sigmundsson F, Parks M, Hooper AJ, Geirsson H, Vogfjörd KS, Drouin V, Ofeigsson B, Hreinsdottir S, Hjaltadottir S, Einarsson P, Jonsdottir K, Barsotti S (2021) Un-stressing of crust prior to eruptions: precursors to the 2021 eruption at Geldingadalir, Mt. Fagradalsfjall, in the Reykjanes Peninsula Oblique Rift, Iceland. In: AGU Fall Meeting 20212

Sigurgeirsson MÁ (1995) The Younger-Stampar eruption at Reykjanes, SW-Iceland. Náttúrufræðingurinn 64:211–230

Spampinato L, Sciotto M, Cannata A, Cannavó F, La Spina A, Palano M, Salerno GG, Privitera E, Caltabiano T (2015) Multiparametric study of the February-April 2013 paroxysmal phase of Mt. Etna New South-East Crater. Geochem Geophys Geosystems 16(6):1932–1949

Sparks RSJ (1978) The dynamics of bubble formation and growth in magmas: a review and analysis. J Volcanol Geotherm Res 3(1):1–37

Swanson DA, Duffield WA, Jackson DB, Peterson DW (1979) Chronological narrative of the 1969-71 Mauna Ulu eruption of Kilauea Volcano, Hawaii. U.S Geol Surv Prof Paper 1056:1056:55

Tanguy JC, Patane G (1984) Activity of Mount Etna, 1977-1983: volcanic phenomena and accompanying seismic tremor. Bull Volcanol 47-2(2)

Tepp G, Hotovec-Ellis A, Shiro B, Johanson I, Thelen W, Haney MM (2020) Seismic and geodetic progression of the 2018 summit caldera collapse of K̄ilauea volcano. Earth Planet Sci Lett 540

Thompson G, McNutt SR, Tytgat G (2002) Three distinct regimes of volcanic tremor associated with the eruption of Shishaldin Volcano, Alaska 1999. Bull Volcanol 64(8):535–547

Thordarson T, Höskuldsson Á (2008) Postglacial volcanism in Iceland. Jökull 58:197–228

Trnkoczy A (2012) Understanding and parameter setting of STA/LTA trigger algorithm. New Manual Seismol Observ Pract 2:1–41

Witt T, Walter TR (2017) Video monitoring reveals pulsating vents and propagation path of fissure eruption during the March 2011 Pu'u 'Ō'ō eruption, Kilauea volcano. J Volcanol Geotherm Res 330:43–55

Zobin VM (2013) Complex monitoring of volcanic activity : methods and results. Nova Science Publishers Inc

Zobin VM (2017) Volcanic tremor. Introduction Volcanic Seismol 4:263–288